Biosensors and Bioelectronics 127 (2019) 188–193

Contents lists available at ScienceDirect

Biosensors and Bioelectronics

journal homepage: www.elsevier.com/locate/bios

MicroRNA detection based on duplex-specific nuclease-assisted target recycling and gold nanoparticle/graphene oxide nanocomposite-mediated electrocatalytic amplification

Yuanyuan Han[a,1], Zhen Qiu[a,1], Ganesh N. Nawale[b], Oommen P. Varghese[b], Jöns Hilborn[b], Bo Tian[a,c,*], Klaus Leifer[a,**]

[a] Department of Engineering Sciences, Uppsala University, Box 534, SE-751 21 Uppsala, Sweden
[b] Department of Chemistry-Ångström, Uppsala University, Box 538, SE-751 21 Uppsala, Sweden
[c] Department of Micro, and Nanotechnology, Technical University of Denmark, DK-2800 Kongens Lyngby, Denmark

ARTICLE INFO

Keywords:
Gold nanoparticles
Graphene oxide
MicroRNA detection
Electrocatalytic amplification
Duplex-specific nuclease

ABSTRACT

DNA technology based bio-responsive nanomaterials have been widely studied as promising tools for biomedical applications. Gold nanoparticles (AuNPs) and graphene oxide (GO) sheets are representative zero- and two-dimensional nanomaterials that have long been combined with DNA technology for point-of-care diagnostics. Herein, a cascade amplification system based on duplex-specific nuclease (DSN)-assisted target recycling and electrocatalytic water-splitting is demonstrated for the detection of microRNA. Target microRNAs can form DNA: RNA heteroduplexes with DNA probes on the surface of AuNPs, which can be hydrolyzed by DSN. MicroRNAs are preserved during the reaction and released into the suspension for the digestion of multiple DNA probes. After the DSN-based reaction, AuNPs are collected and mixed with GO to form AuNP/GO nanocomposite on an electrode for the following electrocatalytic amplification. The utilization of AuNP/GO nanocomposite offers large surface area, exceptional affinity to water molecules, and facilitated mass diffusion for the water-splitting reaction. For let-7b detection, the proposed biosensor achieved a limit detection of 1.5 fM in 80 min with a linear detection range of approximately four orders of magnitude. Moreover, it has the capability of discriminating non-target microRNAs containing even single-nucleotide mismatches, thus holding considerable potential for clinical diagnostics.

1. Introduction

Motivated by the requirements of point-of-care diagnostics, DNA technology based bio-responsive nanomaterials have been widely studied to bring novel properties to different systems of, *e.g.*, biosensing (Liang et al., 2014), imaging (Lee et al., 2014), drug delivery (Chou et al., 2014; Li et al., 2014; Raeesi et al., 2016), and gene therapy (Wang et al., 2018). Among the huge variety of DNA functionalized nanomaterials, DNA modified gold nanoparticles (AuNPs) attract much attention due to their flexible size and net charge, good biocompatibility, specific recognition, predictable enzyme-based reaction, and favorable optical, thermal, electrical and catalytic properties (Giljohann et al., 2010; Rasheed and Sandhyarani, 2017). Induced by the trend of bio-responsive nanomaterials, two-dimensional materials, *e.g.*, graphene oxide (GO) sheets have also been considered promising in biomedical applications because of their extraordinary advantages in surface area, amphiphilicity, mechanical strength, and sensitivity to the local environment changes (Pumera, 2011). Due to the unique properties introduced by AuNPs and GO sheets, many recent advances reveal that AuNP/GO nanocomposites open a new avenue of biosensing applications, *e.g.*, electrochemical sensing for metal ion and DNA (Hu et al., 2011; Wang et al., 2016), surface plasmon resonance sensing for microRNA (Ma et al., 2018), field-effect transistor sensing for protein (Mao et al., 2010), and surface-enhanced Raman spectroscopy for protein and microRNA (Wei et al., 2017).

MicroRNAs, a class of short endogenous noncoding RNA molecules with approximately 19–23 nucleotides, are important biomarkers in the biological processes including tumor initiation and metastasis (Hagen

* Corresponding author at: Department of Micro- and Nanotechnology, DTU, DK-2800 Kongens Lyngby, Denmark.
** Corresponding author.
E-mail addresses: botia@dtu.dk (B. Tian), klaus.leifer@angstrom.uu.se (K. Leifer).
[1] Authors contributed equally to this work.

https://doi.org/10.1016/j.bios.2018.12.027
Received 27 August 2018; Received in revised form 6 December 2018; Accepted 14 December 2018
Available online 22 December 2018
0956-5663/

and Lai, 2008; Lu et al., 2005). Traditional methods for microRNA detection cannot fully meet the demand because of microRNAs' high sequence homology, short sequence length, and low concentrations in body fluids (Shen et al., 2015). To overcome these challenges, various new strategies have been investigated (T. Tian et al., 2015), among which duplex-specific nuclease (DSN)-assisted target recycling (Yin et al., 2012) is highlighted due to its capability of isothermal signal amplification and single-nucleotide mismatch discrimination (Anisimova et al., 2008; Qiu et al., 2015). DSN can hydrolyze the DNA strand in DNA: RNA heteroduplexes but preserves the RNA strand, which means the RNA sequences can be released after the reaction and trigger more DNA cleavage reactions. Compared with traditional methods such as oligonucleotide microarrays, Northern blotting, and quantitative reverse transcription polymerase chain reaction, the DSN-based system is free of the complex design of probes or special instruments. Therefore, DSN-assisted target recycling has been applied for microRNA detection in combination with different sensing technologies, including colorimetric sensors (Wang et al., 2015), fluorescence-based assays (Degliangeli et al., 2014), surface-enhanced Raman scattering-based sensors (Ma et al., 2018), optomagetic readouts (Tian et al., 2017, 2018) and electrochemical sensors (Castañeda et al., 2017; Yang et al., 2014; Zhang et al., 2016). Among these different sensors, electrochemical sensors have advantages with high sensitivity, easy fabrication, and fast responsibility (Kelley et al., 2014), thus being the most widely adopted sensing technology.

Water-splitting reactions are cost-effective and environmentally friendly, which makes them decent signal generation reactions for electrochemical biosensing. An electrocatalytic immunosensor was reported by Zhang et al. based on Pt nanoparticle catalyzed water-splitting reaction, which obtained a detection limit of 1 fg/mL prostate-specific antigen (Zhang et al., 2010). Tian *et al.* reported a DNA detection method using cobalt phosphide-based photocatalytic water-splitting reactions that achieved a detection limit of 100 pM as well as single-base mismatch discrimination (J.Q. Tian et al., 2015). Here, we report a label-free electrochemical biosensor for microRNA detection, which contains a homogeneous target recycling step and a water-splitting measuring step. Triggered by the presence of target microRNA, *i.e.*, let-7b used in this study, the single-stranded DNA probes on the surface of AuNPs are hydrolyzed by DSN, exposing the surface of AuNPs. Thereafter recovered AuNPs are mixed with GO sheets to form AuNP/GO nanocomposite on an indium tin oxide (ITO) electrode. The AuNP/GO-modified electrodes are then utilized to catalyze the water-splitting reaction as the measuring step, resulting in an electrocatalytic signal that is proportional to the exposed area of AuNPs, allowing reliable and accurate quantification of microRNA.

2. Materials and methods

2.1. Chemicals and sequences

Graphene oxide (2 mg/mL, dispersion in H_2O), Gold(III) chloride hydrate (~50% Au basis), sodium citrate dihydrate (≥99%), thiol-PEG (Mw = 2000), $MgCl_2$, PBS buffer (1 M, pH 7.4) and glycerol were purchased from Sigma-Aldrich (St. Louis, USA). RNase inhibitor (20 U/μL) and Tris-HCl (1 M, pH 8.0) buffer were purchased from Thermo Fisher Scientific (Waltham, USA). DSN was purchased from Evrogen (Moscow, Russia) and suspended in 25 mM Tris-HCl (pH 8.0) and 50% glycerol. The reaction buffer for the DSN-assisted target recycling (homogeneous target recycling step) was composed of 50 mM Tris-HCl (pH 8.0) and 20 mM $MgCl_2$. Sequences of microRNAs (let-7a, let-7b, let-7c, let-7d and let-7e) and the DNA probe were synthesized by Biomers (Ulm, Germany) and dissolved in 50 mM Tris-HCl (pH 8.0) for storage. Table 1 shows all sequences of oligonucleotides used in this study.

Table 1
Sequences of oligonucleotides used in this study.

Name[a]	Sequence (5′→3′)
let-7a	uga ggu agu agg uug u**a**u **a**gu u
let-7b	uga ggu agu agg uug ugu ggu u
let-7c	uga ggu agu agg uug u**a**u ggu u
let-7d	**a**ga ggu agu agg uug **ca**u **a**gu u
let-7e	uga ggu ag**g** agg uug u**a**u **a**gu u
probe	AAC CAC ACA ACC TAC TAC CTC ATT T-C3-thiol

[a] The DNA sequence is written in uppercase letters while RNAs are written in lowercase letters. In let-7a, c, d and e, the bases that differ from those in let-7b are **bold and underlined**.

2.2. Apparatus

All of the electrochemical measurements were performed in a three-electrode configuration on CHI 760C electrochemical workstation (CH Instruments, USA) at room temperature. Modified indium tin oxide (ITO, 15 Ω), platinum wire and Ag/AgCl (3 M KCl) were used as the working, counter and reference electrodes, respectively.

2.3. Preparation and modification of AuNPs

AuNPs were prepared using a citrate reduction method and functionalized by thiol-probes using a pH-assistant method (Zhang et al., 2012). Briefly, citrate-HCl buffer (100 mM, pH 3) was added into the AuNPs and thiol-probe solution in several steps. The ratio of AuNP: probe was 1:2000. Single-stranded DNA probes self-assembled on the AuNPs surface stably by sulfur-gold interactions (Bhatt et al., 2011). Thereafter, thiol-PEG (3 mg/mL) was added to the suspension to block the uncapped surface of AuNPs. After that, Probe-AuNPs were collected by 3 times of centrifugation (13,000 r/min for 10 min, Hitachi Koki Co., Japan) purified by washing. Prepared probe-AuNPs were suspended in 50 mM Tris-HCl (pH 8.0) buffer solution for storage at 4 °C.

2.4. DSN-assisted target recycling

For the DSN-assisted target recycling, 5 μL of probe-AuNPs (6 mg/mL), 2.5 μL of RNase inhibitor (20 U/μL), 1 μL of DSN (1 U/μL), and 91.5 μL of sample (containing analyte) were mixed and incubated at 50 °C for 1 h to perform DSN-assisted target recycling. After the incubation, AuNPs were collected by twice of centrifugation (6500 r/min for 5 min) purified by washing. The collected AuNPs were resuspended in 95 μL of deionized water and sonicated with 5 μL of GO (2 mg/mL) for 2 min. The concentrations of AuNPs and GO in the catalyst suspension were 0.3 and 0.1 mg/mL, respectively.

2.5. Electrocatalytic detection

For the electrocatalytic amplification-based measuring step, 5 μL of the catalyst suspension (containing AuNPs and GO) was pipetted to the surface of ITO (1 cm × 0.5 cm) and dried at 60 °C for 1 min. The electrocatalytic activity of the AuNP/GO nanocomposite for water-splitting was characterized by amperometric i-t-tests at −1 V vs Ag/AgCl (3 M KCl) in an electrolyte of PBS (1 M, pH 7.4) for 300 s. All measurements were performed 3 times independently and the standard errors were plotted as error bars.

2.6. DLS and SEM characterization

The hydrodynamic sizes of AuNPs and probe-AuNPs were characterized by dynamic light scattering (DLS). DLS measurements were performed in Zetasizer Nano ZSP (Malvern Panalytical, Malvin, UK) with a He-Ne 633 nm laser (Max 10 mW). The morphology and nanostructure of the AuNP/GO were obtained by field emission scanning

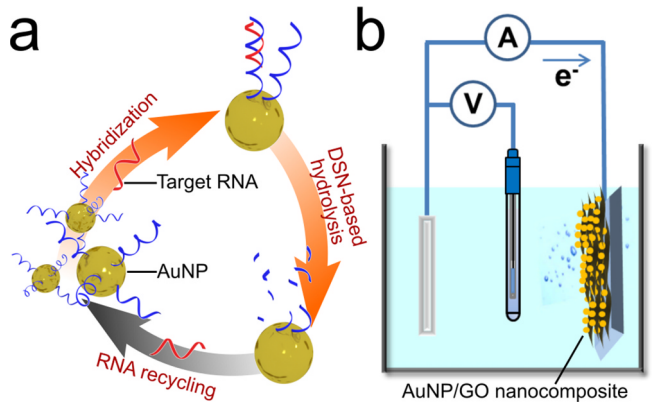

Fig. 1. Schematic illustration of (a) the working principle of AuNP surface exposure based on DSN-assisted target recycling, and (b) the three-electrode configuration for the electrocatalytic detection using AuNP/GO-modified electrodes.

electron microscopy (Merlin FE-SEM, Zeiss, Germany) at 15 kV, using an in-lens secondary electron detector.

3. Results and discussion

3.1. Detection principle

The AuNP/GO nanocomposite-based biosensing strategy is composed of two amplification steps, *i.e.*, DSN-assisted target recycling for exposing AuNP surface and AuNP-based electrocatalytic amplification for signal generation. AuNPs used in this biosensing platform were functionalized with single-stranded DNA probes, which have the complementary sequence to the target RNA. Through the Au-S based conjugation, DNA probes form a DNA layer that covers the entire surface of the AuNPs, thus reducing the area of H_2O adsorption sites in the following electrocatalytic reaction. In the step of DSN-based AuNP surface recovery (schematically illustrated in Fig. 1a), target microRNAs hybridize with the DNA probes on the surface of AuNPs, forming DNA: RNA heteroduplexes that can be hydrolyzed by DSN. The DNA components in the heteroduplexes were hydrolyzed, exposing the surface of AuNPs. MicroRNAs were preserved during the DSN-based reaction and thereafter released into the suspension to trigger the hydrolysis of multiple DNA probes, concomitantly exposing more surface areas of AuNPs.

The electrocatalytic amplification step is performed in a three-electrode configuration using AuNP/GO nanocomposite-functionalized electrode for water-splitting (Fig. 1b). The three-dimensional (3D) networks of AuNP/GO nanocomposite significantly increases the number of AuNPs connected to the electrode as compared to a flat substrate, thus increasing the surface area of AuNPs exposed to the electrolyte. AuNPs as the main reactive sites play an important role in the electrocatalytic amplification step for the current signal generation. With various exposed AuNP surface areas, the AuNP/GO-modified electrodes show different catalytic reactivity. In the reaction path of hydrogen evolution reaction, water molecules accept electrons to form OH^-, along with the formation of H_{ad} (hydrogen adsorption) intermediate on AuNPs (Bockris and Potter, 1952). The H_{ad} intermediates recombine to form H_2 on the AuNP/GO-modified electrode (Subbaraman et al., 2012). The intensity of hydrogen generation can be reflected by the recorded current. A larger exposed surface area of AuNPs results in more active sites for hydrogen generation, thus markedly improving the corresponding current signal. Additionally, the porous GO structure provides efficient mass transfer pathways. According to the extended definition of amplification, both the above-mentioned steps (*i.e.*, one single let-7b can be cycled to trigger multiple cutting reactions, and the area of AuNP surface recovered by one single cutting reaction catalyzes multiple H_2O molecules) are amplifications (Blaedel and Boguslaski, 1978). Therefore, the proposed biosensing strategy can be regarded as a cascade amplification strategy.

3.2. Feasibility test

Nanostructures of AuNPs, GO sheets and the hybrid structures such as AuNP/GO multilayers with gold nanoparticles inserting between GO sheets were confirmed by SEM. AuNPs used in this study are well dispersed before mixing with GO (Fig. 2a). The cross-sectional morphology of the AuNP/GO nanocomposite is shown in Fig. 2b. AuNPs are dispersed and cladded between GO sheets, thus forming a 3D framework on the ITO electrode. Four different kinds of ITO-based electrodes, *i.e.*, the naked electrode, the GO-modified electrode, the AuNP-modified electrode, and the AuNP/GO-modified electrode, were prepared and investigated as the cathodic electrode for the electrocatalytic reaction. The i-t curves of these electrodes can be seen in Fig. 2c. The AuNP/GO-modified electrode presented a current that decreased as a function of reaction time but transformed into a faradic steady-state after *ca.* 180 s. Therefore, we chose the current at 200 s to represent the performance of the electrode in the following study. As expected, the AuNP/GO-modified electrode manifested the highest current (red curve in the plot). The AuNP-electrode provided the second highest output signal (blue curve in the plot) due to the catalytic activity of Au. The GO-modified electrode obtained a current signal slightly higher than that obtained by the naked ITO electrode (cf. black and yellow curves in the plot), which was caused by the large surface area and good H_2O affinity of GO

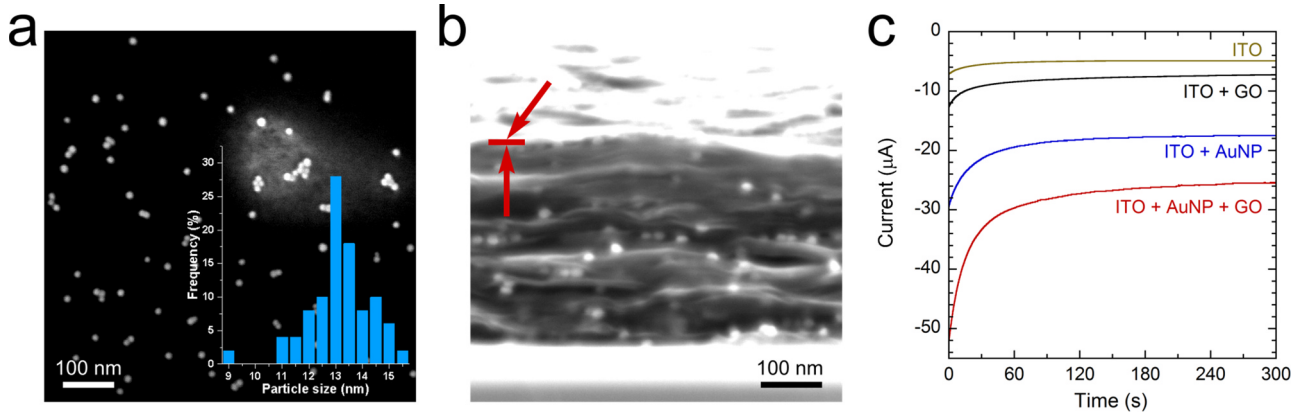

Fig. 2. Representative SEM images of (a) individual AuNPs dispersed on the SiO_2/Si substrate (insert shows the size distribution of AuNPs), and (b) the cross-section of AuNP/GO nanocomposite. Red arrows indicate the edge of the AuNP/GO nanocomposite thin film cross-section. (c) The i-t curves of water-splitting reactions using the naked ITO electrode and ITO electrodes functionalized with different materials.

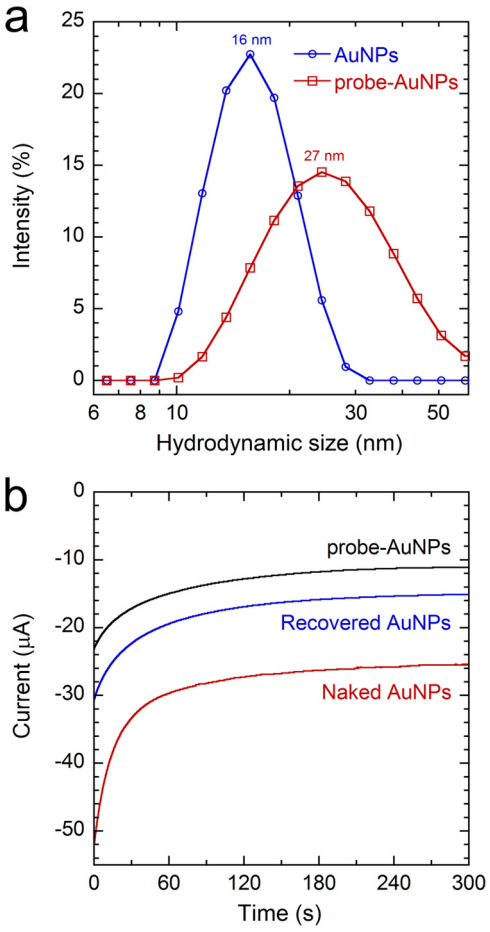

Fig. 3. (a) DLS measurement for hydrodynamic radius distribution of AuNPs and probe-AuNPs. (b) The i-t curves of water-splitting reactions using $AuNP_{naked}$/GO-modified, $AuNP_{probe}$/GO-modified, and $AuNP_{recovered}$/GO-modified electrodes, respectively.

sheets. Besides the large surface area, the 3D nanostructure of AuNP/GO nanocomposite also facilitates the mass diffusion (Wei et al., 2013), resulting in another positive contribution to the performance of AuNP/GO-modified electrodes.

The thiol-modified single-stranded DNA probe, which contains a sequence complementary to the target RNA, was utilized for the AuNP functionalization. After conjugation of DNA probes, the hydrodynamic radius of AuNPs increased to *ca.* 10 nm (cf. DLS results in Fig. 3a), corresponding to the length of the probe. However, due to the DNA probe conjugation, the size distribution of probe-AuNPs was larger than that of naked AuNPs, implying a less monodisperse colloidal system. The output catalytic current obtained by the $AuNP_{probe}$/GO-modified electrode was much smaller than the current obtained by the $AuNP_{naked}$/GO-modified electrode (cf. black and red curves in Fig. 3b), demonstrating the formation of the DNA probe layer on the surface of AuNP. In the presence of target microRNA, DSN-assisted target recycling reaction hydrolyzes the DNA probe layer, thus recovering the surface of AuNPs for catalyzing the cathodic water splitting reaction. Therefore, the $AuNP_{recovered}$/GO-modified electrode offered a higher catalytic current than that provided by the $AuNP_{probe}$/GO-modified electrode (cf. blue and black curves in Fig. 3b). We observed that the catalytic current could not be totally recovered to the level of using $AuNP_{naked}$/GO-modified electrode, which was caused by the utilization of thiol-PEG and the residual of DNA probes after the hydrolyzation reaction. In addition to the surface exposure, rupture of the DNA probe layer directly increased the electrons tunneling probability between AuNPs and GO scaffold, which also contributes to the increase of

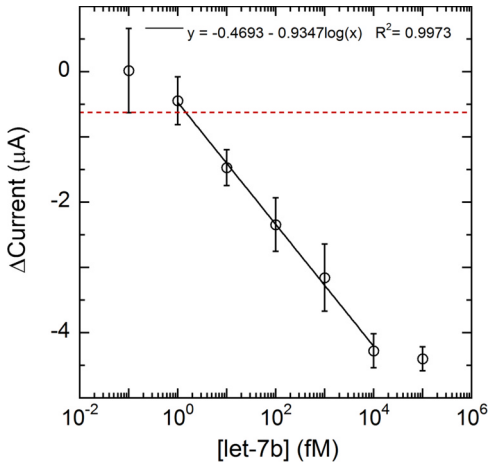

Fig. 4. Dose-response curve for let-7b quantification. The red dash line and the black solid line indicate the cut-off value and linear detection range, respectively. (For interpretation of the references to color in this figure legend, the reader is referred to the web version of this article.)

catalytic current. Contributions of surface exposure and tunneling probability increase were not distinguished in the current work but will be investigated in future studies.

3.3. Quantification of microRNA

To demonstrate the quantitative relationship between the concentration of target microRNA and the water-splitting reaction current, serial concentrations of target microRNA (let-7b) were measured by the proposed cascade amplification system. Target concentrations ranging from 0.1 fM to 100 pM were reacted with the probe-AuNPs and DSN at 50 °C. After DSN-assisted target recycling, AuNPs were collected to prepare the AuNP/GO-modified electrode for the following electrocatalytic amplification step. The catalytic current increase ($\Delta I = I_{sample} - I_{blank}$, where I_{blank} is the average current signal of blank control samples) recorded at 200 s was chosen as the output signal for the dose-response curve (Fig. 4). The dose-response curve shows a monotonous current increase with the increase of target concentration. A linear correlation between current and logarithm concentration is obtained at the range of 1 fM −10 pM. The limit of detection (LOD), calculated based on the 3σ criterion, is 1.5 fM of let-7b. Compared to most of the DSN-based microRNA detection systems that employ one single amplification step (*i.e.*, DSN-assisted target recycling) (Castañeda et al., 2017; Tran et al., 2013; Yang et al., 2014; Zhang et al., 2016), the proposed AuNP/GO-based biosensor is more sensitive due to the design of cascade amplification (*i.e.*, DSN-assisted target recycling followed by an electrocatalytic amplification). However, many other cascade amplification-based microRNA detection systems have achieved much lower LODs of, *e.g.*, 6.8 (Bo et al., 2018), 8 (Zhang et al., 2014), 11 (Yuan et al., 2018) and 25.1 aM (Yu et al., 2018), implying higher efficiencies of their cascade amplification designs. We hold the opinion that the 1.5 fM LOD is sufficient for most of the current studies of microRNA. The concentration of microRNA differs in different body fluid. The concentration of total let-7 in plasma is about 100 fM (Williams et al., 2013). Another study reported that the let-7b concentrations of the urine samples from kidney cancer patients ranged from 1.835 fM to 6.160 fM (Fedorko et al., 2017). Additionally, current microRNA detections are usually performed for cell extracts, in which microRNAs are much more concentrated and pure (much fewer matrix effects). For comparison, the detection limits of commercialized fluorescence-based microRNA assays (Qubit and Quant-iT microRNA assays, Thermo Fisher, USA) are at the sub-nano to nanomolar level.

Since DTT (dithiothreitol) can trigger AuNP aggregation, we avoided its use in our method. However, DTT was always added into

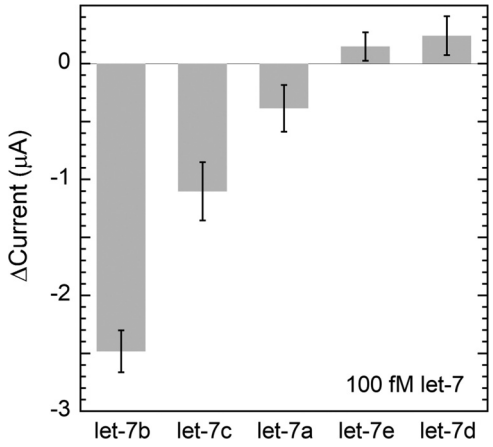

Fig. 5. Specificity test using five different let-7 microRNAs. Five members of the let-7 family, *i.e.*, let-7a, let-7b, let-7c, let-7d and let-7e, were measured by the proposed biosensor at a concentration of 100 fM.

the reaction buffer to maintain DSN activity in previous DSN-based biosensors, which means the efficiency of our DSN may be lower than expected. To investigate the influence of DTT, we performed DSN reactions with and without DTT protection and compared the reaction efficiency by gel electrophoresis. Analysis of the polyacrylamide gel electrophoresis indicated that all DNA: RNA heteroduplex were hydrolyzed in both reactions, implying that 1 U of DSN was sufficient for the proposed method without DTT (data not shown). Although the usage of DTT has been avoided in this study, AuNP aggregation was still observed, which lowered the efficiency of the proposed cascade amplification strategy. It was reported that Mg^{2+} could lead to AuNP aggregation (Pamies et al., 2014), which was controlled by the utilization of thiol-PEG in this study but still influenced the homogeneity of the AuNP/GO nanocomposites. Moreover, surface recovered AuNPs easily absorb biomacromolecules, thus limiting their robustness against matrix effects. These limitations as well as the optimization of the homogeneity of the electrode surfaces will be the topic of our future studies.

Repeatability of AuNP/GO nanocomposite-coated ITO electrodes is vital for the proposed biosensor. Currently, for simplicity, we chose a drop-drying method to coat nanocomposites onto ITO, which was not optimal. To increase the homogeneity of functionalized ITO electrodes, spin coating will be a good option for electrode preparation. In the spin coating strategy, nanocomposites can be rotated at a selected speed to spread the coating material by a suitable centrifugal force, which is beneficial to choose a similar weight of AuNP/GO nanocomposite for a uniform film. Moreover, since the catalytic reaction mainly occurs on the surfaces, it is possible to adjust the thickness of the film by viscosity and concentration of the solution to improve the electrocatalytic performance of the proposed biosensor.

3.4. Specificity test

Due to the high sequence homology among microRNAs of the same family, a specificity test is challenging in microRNA analysis (Baker, 2010; Shen et al., 2015). To demonstrate the specificity of the proposed biosensor, five members of the let-7 family, *i.e.*, let-7a, let-7b, let-7c, let-7d and let-7e, were measured. Sequences of these let-7 microRNAs are shown in Table 1, in which we can see that let-7c has single-nucleotide mismatch compared with the target, let-7b; while let-7a, let-7d, let-7e has double- or several-nucleotides mismatches. All the microRNAs were detected at a concentration of 100 fM (Fig. 5). For the DSN-assisted target recycling, a perfect matched DNA: RNA heteroduplex sequence of at least 15 base pairs are needed to trigger the hydrolysis (Qiu et al., 2015), therefore let-7a and let-7c showed nonspecific signals because of their 16-bp-long perfect match with the DNA probe (designed for let-7b). For the detection of 100 fM of let-7a and let-7c, nonspecific signals were observed which was equal in magnitude to the signal of 0.8 fM and 4.8 fM of let-7b, respectively, demonstrating a high specificity of the proposed biosensor that can discriminate even single-nucleotide mismatches. Moreover, we observed that let-7d and let-7e showed signals lower than the signal of blank control samples, which was caused by the formation of a stable (*i.e.*, cannot be hydrolyzed by DSN) DNA: RNA heteroduplex layer on the surface of AuNPs. Compared with the single-stranded DNA probe layer, the stable DNA: RNA heteroduplex layer further lowered the tunneling probability at the interface between the AuNP and the GO in the AuNP/GO nanocomposite, therefore performing output currents lower than the signal of blank control samples.

4. Conclusion

In summary, a cascade amplification strategy based on DSN-assisted target recycling and an electrocatalytic reaction were demonstrated for microRNA detection. DSN-assisted target recycling was utilized to rupture the single-stranded DNA probes on the surface of AuNPs, recovering the surface for the following water-splitting reaction. The utilization of AuNP/GO nanocomposite offered large surface area, efficient water affinity, good conductivity and facilitated mass diffusion for the electrocatalytic reaction. An LOD of 1.5 fM of let-7b was achieved in a total assay time of 80 min with a linear detection range of approximately four orders of magnitude. The proposed biosensor was also demonstrated to discriminate non-target microRNAs containing even single-nucleotide mismatches.

CRediT authorship contribution statement

Yuanyuan Han: Conceptualization, Data curation, Funding acquisition, Investigation, Writing - original draft, Software, Validation. **Zhen Qiu:** Conceptualization, Investigation, Methodology, Visualization, Writing - original draft. **Ganesh N. Nawale:** Data curation, Validation, Writing - review & editing. **Oommen P. Varghese:** Data curation, Validation, Writing - review & editing. **Jöns Hilborn:** Formal analysis, Supervision, Writing - review & editing. **Bo Tian:** Conceptualization, Formal analysis, Funding acquisition, Methodology, Supervision, Visualization, Writing - review & editing. **Klaus Leifer:** Formal analysis, Funding acquisition, Project administration, Resources, Supervision, Writing - review & editing.

Acknowledgments

This work was financially supported by the Vetenskapsrådet of Sweden (grant no. 2016–05259), Knut and Alice Wallenberg Foundation, China Scholarship Council (201404910509) and H2020 Marie Skłodowska-Curie Actions (grant no. 713683, COFUNDfellowsDTU).

Declaration of interests

None.

References

Anisimova, V.E., Rebrikov, D.V., Shagin, D.A., Kozhemyako, V.B., Menzorova, N.I., Staroverov, D.B., Ziganshin, R., Vagner, L.L., Rasskazov, V.A., Lukyanov, S.A., Shcheglov, A.S., 2008. BMC Biochem. 9 (1), 14.
Baker, M., 2010. Nat. Methods 7, 687–692.
Bhatt, N., Huang, P.-J.J., Dave, N., Liu, J., 2011. Langmuir 27 (10), 6132–6137.
Blaedel, W.J., Boguslaski, R.C., 1978. Anal. Chem. 50 (8), 1026–1032.
Bo, B., Zhang, T., Jiang, Y., Cui, H., Miao, P., 2018. Anal. Chem. 90 (3), 2395–2400.
Bockris, J.O.M., Potter, E.C., 1952. J. Electrochem. Soc. 99 (4), 169–186.
Castañeda, A.D., Brenes, N.J., Kondajji, A., Crooks, R.M., 2017. J. Am. Chem. Soc. 139 (22), 7657–7664.

Chou, L.Y.T., Zagorovsky, K., Chan, W.C.W., 2014. Nat. Nanotechnol. 9 (2), 148–155.
Degliangeli, F., Kshirsagar, P., Brunetti, V., Pompa, P.P., Fiammengo, R., 2014. J. Am. Chem. Soc. 136 (6), 2264–2267.
Fedorko, M., Juracek, J., Stanik, M., Svoboda, M., Poprach, A., Buchler, T., Pacik, D., Dolezel, J., Slaby, O., 2017. Bioch. Med. 27 (2), 411–417.
Giljohann, D.A., Seferos, D.S., Daniel, W.L., Massich, M.D., Patel, P.C., Mirkin, C.A., 2010. Angew. Chem. Int. Ed. 49 (19), 3280–3294.
Hagen, J.W., Lai, E.C., 2008. Cell Cycle 7 (15), 2327–2332.
Hu, Y., Hua, S., Li, F., Jiang, Y., Bai, X., Li, D., Niu, L., 2011. Biosens. Bioelectron. 26 (11), 4355–4361.
Kelley, S.O., Mirkin, C.A., Walt, D.R., Ismagilov, R.F., Toner, M., Sargent, E.H., 2014. Nat. Nanotechnol. 9 (12), 969–980.
Lee, K., Cui, Y., Lee, L.P., Irudayaraj, J., 2014. Nat. Nanotechnol. 9 (6), 474–480.
Li, Z.H., Dong, K., Huang, S., Ju, E.G., Liu, Z., Yin, M.L., Ren, J.S., Qu, X.G., 2014. Adv. Funct. Mater. 24 (23), 3612–3620.
Liang, H., Zhang, X.-B., Lv, Y., Gong, L., Wang, R., Zhu, X., Yang, R., Tan, W., 2014. Acc. Chem. Res. 47 (6), 1891–1901.
Lu, J., Getz, G., Miska, E.A., Alvarez-Saavedra, E., Lamb, J., Peck, D., Sweet-Cordero, A., Ebert, B.L., Mak, R.H., Ferrando, A.A., Downing, J.R., Jacks, T., Horvitz, H.R., Golub, T.R., 2005. Nature 435 (7043), 834–838.
Ma, D., Huang, C., Zheng, J., Tang, J., Li, J., Yang, J., Yang, R., 2018. Biosens. Bioelectron. 101, 167–173.
Mao, S., Lu, G., Yu, K., Bo, Z., Chen, J., 2010. Adv. Mater. 22 (32), 3521–3526.
Pamies, R., Cifre, J.G.H., Espín, V.F., Collado-González, M., Baños, F.G.D., García de la Torre, J., 2014. J. Nanopart. Res. 16 (4), 2376.
Pumera, M., 2011. Mater. Today 14 (7–8), 308–315.
Qiu, X., Zhang, H., Yu, H., Jiang, T., Luo, Y., 2015. Trends Biotechnol. 33 (3), 180–188.
Raeesi, V., Chou, L.Y., Chan, W.C.W., 2016. Tuning the drug loading and release of DNA-assembled gold-nanorod superstructures. Adv. Mater. 28 (38), 8511–8518.
Rasheed, P.A., Sandhyarani, N., 2017. Microchim. Acta 184 (4), 981–1000.
Shen, Y., Tian, F., Chen, Z., Li, R., Ge, Q., Lu, Z., 2015. Biosens. Bioelectron. 71, 322–331.
Subbaraman, R., Tripkovic, D., Chang, K.-C., Strmcnik, D., Paulikas, A.P., Hirunsit, P., Chan, M., Greeley, J., Stamenkovic, V., Markovic, N.M., 2012. Nat. Mater. 11, 550.
Tian, B., Ma, J., Qiu, Z., Zardán Gómez de la Torre, T., Donolato, M., Hansen, M.F., Svedlindh, P., Strömberg, M., 2017. ACS Nano 11 (2), 1798–1806.
Tian, B., Qiu, Z., Ma, J., Donolato, M., Hansen, M.F., Svedlindh, P., Strömberg, M., 2018. ACS Appl. Mater. Inter. 10 (3), 2957–2964.
Tian, J.Q., Chen, N.Y., Liu, Q., Xing, W., Sun, X.P., 2015a. Angew. Chem. Int. Ed. 54 (18), 5493–5497.
Tian, T., Wang, J., Zhou, X., 2015b. Org. Biomol. Chem. 13 (8), 2226–2238.
Tran, H.V., Piro, B., Reisberg, S., Duc, H.T., Pham, M.C., 2013. Anal. Chem. 85 (17), 8469–8474.
Wang, D., Liu, Q., Wu, D., He, B., Li, J., Mao, C., Wang, G., Qian, H., 2018. ACS Appl. Mater. Interfaces 10 (18), 15504–15516.
Wang, N., Lin, M., Dai, H., Ma, H., 2016. Biosens. Bioelectron. 79, 320–326.
Wang, Q., Li, R.-D., Yin, B.-C., Ye, B.-C., 2015. Analyst 140 (18), 6306–6312.
Wei, M., Maozhong, S., Pan, F., Si, L., Liguang, X., Hua, K., Chuanlai, X., 2017. Adv. Mater. 29 (42), 1703410.
Wei, W., Shubin, Y., Haixin, Z., Ingo, L., Xinliang, F., Klaus, M., 2013. Adv. Mater. 25 (21), 2909–2914.
Williams, Z., Ben-Dov, I.Z., Elias, R., Mihailovic, A., Brown, M., Rosenwaks, Z., Tuschl, T., 2013. Proc. Natl. Acad. Sci. USA 110, 4255–4260.
Yang, C., Dou, B., Shi, K., Chai, Y., Xiang, Y., Yuan, R., 2014. Anal. Chem. 86 (23), 11913–11918.
Yin, B.-C., Liu, Y.-Q., Ye, B.-C., 2012. J. Am. Chem. Soc. 134 (11), 5064–5067.
Yu, S., Wang, Y., Jiang, L.-P., Bi, S., Zhu, J.-J., 2018. Anal. Chem. 90 (7), 4544–4551.
Yuan, Y.-H., Chi, B.-Z., Wen, S.-H., Liang, R.-P., Li, Z.-M., Qiu, J.-D., 2018. Biosens. Bioelectron. 102, 211–216.
Zhang, J., Ting, B.P., Khan, M., Pearce, M.C., Yang, Y., Gao, Z., Ying, J.Y., 2010. Biosens. Bioelectron. 26 (2), 418–423.
Zhang, J., Wu, D.-Z., Cai, S.-X., Chen, M., Xia, Y.-K., Wu, F., Chen, J.-H., 2016. Biosens. Bioelectron. 75, 452–457.
Zhang, X., Servos, M.R., Liu, J., 2012. J. Am. Chem. Soc. 134 (17), 7266–7269.
Zhang, X., Wu, D., Liu, Z., Cai, S., Zhao, Y., Chen, M., Xia, Y., Li, C., Zhang, J., Chen, J., 2014. Chem. Commun. 50 (82), 12375–12377.